

COVER PAGE

Document downloaded by @DAEL

Fri Nov 27 19:53:13 2026
For personal use

When automatic English translation is provided, only the original document is authentic.
The EAA cannot be held responsible of any translation error

Bibliographical reference

Photoacoustics in a Cylindrical Resonator Containing a Flowing Gas, M. Willatzen, B. Lassen and Y. Feng, Acta Acustica **vol. 96** (Number 5), 2010, pp. 797-806

DOI
https://doi.org/10.3813/AAA.918337

Acta Acustica united with Acustica
Vol. 96 (2010) 797 – 806

Scientific Papers
DOI 10.3813/AAA.918337

Photoacoustics in a Cylindrical Resonator Containing a Flowing Gas

M. Willatzen, B. Lassen, Y. Feng
Mads Clausen Institute for Product Innovation, University of Southern Denmark, Alsion 2, 6400 Sønderborg, Denmark. willatzen@mci.sdu.dk

Summary
A detailed study of photoacoustics in circular resonators and waveguides in the presence of a gas flow is presented based on the Green's function method. In the first part of the paper, a wave equation is derived describing sound propagation in a flowing (perfect) gas due to a localized heating source. Analytical results are obtained for the acoustic pressure in the case of a constant gas flow subject to different boundary conditions. In the second part of the paper, the derived wave equation is solved for a parabolic flow profile using the finite-element method and results are compared with the constant-flow case. It is demonstrated that the gas-flow profile does not change the pattern of acoustic resonance frequencies significantly. In particular it is noted that the presence of flow gives rise to new peaks and we show that non-linearities with respect to the mean flow velocity appear already at 1% of the speed of sound at certain frequencies.

PACS no. 43.20.-f, 43.58.-e

1. Introduction

The excitation of pressure waves in cavities due to the photoacoustic effect is a very accurate way of determining the concentration of select gases in a flowing fluid. Areas of application include the monitoring of impurities in for example exhaust gasses or oil contamination in compressor, the determination of fermentation of crops during storage, and human health monitoring via breath monitoring[1], to name just a few. Several investigations of photoacoustic excitations in cavities have been carried out for weakly absorbing gasses, different cavity geometries, and laser-beam profiles [2, 3, 4, 5, 6]. Cox *et al.* [6] recently presented an analysis using k-space methods to obtain pulsed photoacoustic fields in gass. This analysis is based on obtaining an expression for the Green's function of the linear wave equation [7]:

$$\vec{\nabla}^2 p - \frac{1}{c^2}\frac{\partial^2 p}{\partial t^2} = -\frac{\beta}{c_p}\frac{\partial H}{\partial t}, \qquad (1)$$

where c is the sound speed, β is the volume thermal expansivity, c_p is the specific heat capacity, and H is the heat energy per unit volume per unit time deposited in the gas. For a pulsed and shaped laser beam, H is a (narrow) function of space and time. The use of Green's functions allows for numerical efficient computation of the photoacoustic generated pressure field for rather general cavity geometries, cavity boundary conditions, and laser-beam profiles and dynamics.

Received 13 August 2009,
accepted 15 April 2010.

While equation (1) applies to the case where viscous effects and thermal conductivity are negligible in the absence of gas flow, we start out by deriving a photoacoustic equation accounting for small viscous and thermal-conduction effects in the presence of a small background gas flow. The model is subsequently solved using the Green's function method. Several case studies are carried out for the case of cylindrical cavities with rigid peripheral cylinder walls considering laser-beam profiles dependent on the radial and axial coordinates, see Figure 1. However, the method can be easily generalized to other waveguide and cavity geometries. We compute photoacoustic pressures for an infinite cylindrical waveguide and a finite cylindrical cavity of axial length L with either rigid or pressure-release axial boundaries. A discussion is presented for the influence of a constant background flow velocity on photoacoustic pressure fields in an (infinite) waveguide. It is demonstrated that a background flow modifies the acoustic pressure and hence has important implications for photoacoustic device applications such as gas spectrometry analysis [8, 9]. A detailed and related discussion of the influence of a background flow for acoustic pressure fields in waveguides in the absence of photoacoustic excitation can be found in, e.g., [10, 11, 12, 13].

Finally, we verify our quasi-analytical Green's function results vs. numerically more elaborate finite-element-method results and present a discussion of the influence of a background flow profile (i.e., where the flow velocity is a function of the radial coordinate) on photoacoustic pressure fields.

© S. Hirzel Verlag · EAA

2. Theory

Consider a flowing gas subject to photoacoustic excitation. Expressions for the pressure, mass density, temperature, entropy separated into static and acoustic contributions read

$$\begin{aligned} p(\vec{r},t) &= p_0 + \tilde{p}, \qquad T(\vec{r},t) = T_0 + \tilde{T}, \\ \rho(\vec{r},t) &= \rho_0 + \tilde{\rho}, \qquad S(\vec{r},t) = S_0 + \tilde{S}, \\ \vec{u}(\vec{r},t) &= \vec{u}_0 + \vec{\tilde{u}}, \end{aligned} \tag{2}$$

where p, T, ρ, S, $\vec{u}$ are the total pressure, temperature, mass density, entropy, particle velocity, p_0, T_0, ρ_0, S_0, $\vec{u}_0$ are the reference pressure, temperature, mass density, entropy, particle velocity, and $\tilde{p}$, $\tilde{T}$, $\tilde{\rho}$, $\tilde{S}$, $\vec{\tilde{u}}$ are the acoustic pressure, temperature, mass density, entropy, particle velocity. We shall in the following restrict our analysis to linear acoustics and neglect any effects caused by second- or higher-order terms in acoustic quantities. The linear acoustic equations can be written as [7]

$$\frac{\mathrm{D}\tilde{\rho}}{\mathrm{D}t} + \rho_0 \vec{\nabla}\cdot\vec{\tilde{u}} = 0, \tag{3}$$

$$\rho_0 \frac{\mathrm{D}\vec{\tilde{u}}}{\mathrm{D}t} = -\vec{\nabla}\tilde{p} + \left(\eta + \frac{4}{3}\mu\right)\vec{\nabla}\vec{\nabla}\cdot\vec{\tilde{u}} - \mu\vec{\nabla}\times\vec{\nabla}\times\vec{\tilde{u}}, \tag{4}$$

$$T_0 \frac{\mathrm{D}\tilde{S}}{\mathrm{D}t} = \frac{K}{\rho_0}\vec{\nabla}^2\tilde{T} + \epsilon. \tag{5}$$

The latter equation (5) can be recast as

$$\frac{\mathrm{D}}{\mathrm{D}t}\left(\tilde{p} - \frac{p_0}{T_0}\tilde{T}\right) = \frac{1}{\gamma}\frac{\mathrm{D}\tilde{p}}{\mathrm{D}t} - \frac{p_0 K}{c_p \rho_0 T_0}\vec{\nabla}^2\tilde{T} - \frac{p_0}{c_p T_0}\epsilon, \tag{6}$$

upon use of the thermodynamic constitutive relation (perfect gas assumption),

$$\tilde{S} = c_p\left(\frac{\tilde{T}}{T_0} - \frac{\gamma-1}{\gamma}\frac{\tilde{p}}{p_0}\right). \tag{7}$$

In deriving the above expression, the derivative

$$\frac{\mathrm{D}}{\mathrm{D}t} = \frac{\partial}{\partial t} + \vec{u}_0\cdot\vec{\nabla}, \tag{8}$$

is introduced, and μ, η, γ, K, ϵ are the shear viscosity, bulk viscosity, ratio of specific heats at constant pressure and volume ($\equiv c_p/c_v$), heat conductivity, and heat energy per unit mass introduced into the gas, respectively. In writing equation (6), we have neglected a contribution to heating caused by viscous effects.

A zeroth-order expression for the acoustic temperature can be found from equation (6),

$$\frac{\partial\tilde{T}}{\partial t} = \frac{(\gamma-1)\,T_0}{\gamma p_0}\frac{\partial\tilde{p}}{\partial t} + \frac{\epsilon}{c_p}, \tag{9}$$

obtained by neglecting the small influence of a background flow $\vec{u}_0$ and heat conduction in the energy equation. Inserting this zeroth-order expression for the acoustic temperature in the heat-conduction term of equation (6) and

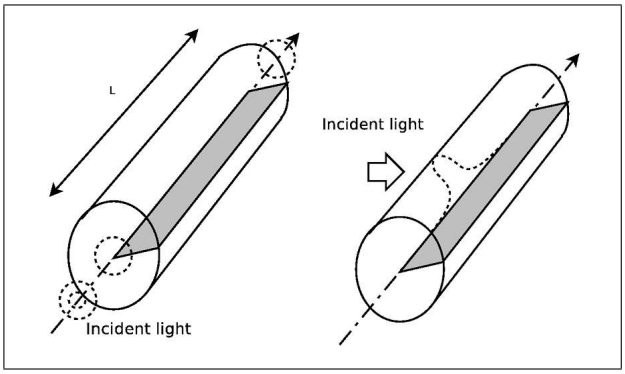

Figure 1. Schematic picture of the cylindrical pipe. (Left) Picture showing the case where the intensity of light is only dependent on the radial coordinate. (Right) Picture showing the case where the intensity of light only depends on the axial coordinate.

combining with equations (3)–(4) leads to (here, and in the following, we assume monofrequency excitation conditions: $\partial/\partial t = \mathrm{i}\omega$ and neglect second-order terms in small quantities: l_v^2, l_h^2, $l_v l_h$, u_0^2, $l_v u_0$, $l_h u_0$ as these are small),

$$\begin{aligned} &\vec{\nabla}^2\tilde{p} + \frac{\omega^2}{c^2}(1-A)\,\tilde{p} - \frac{2\mathrm{i}\omega u_0}{c^2}\frac{\partial\tilde{p}}{\partial z} \\ &= \frac{p_0\gamma}{T_0 c_p c}\left[l_v - l_h\right]\vec{\nabla}^2\epsilon - \frac{p_0\gamma}{T_0 c_p c^2}(1-A)\left[\mathrm{i}\omega\epsilon + u_0\frac{\partial\epsilon}{\partial z}\right], \end{aligned} \tag{10}$$

where the viscous-length and heat-length scales,

$$l_v = \frac{\eta + \frac{4}{3}\mu}{\rho_0 c}, \qquad l_h = \frac{K}{\rho_0 c_p c}, \tag{11}$$

have been used, and

$$A = \mathrm{i}\omega\left[\frac{(\gamma-1)l_h}{c} + \frac{l_v}{c}\right], \tag{12}$$

where c is the medium speed of sound and the background flow velocity u_0 is assumed to be directed along the z axis. Also the constitutive relation

$$\tilde{\rho} = \frac{\rho_0}{p_0}\tilde{p} - \frac{\rho_0}{T_0}\tilde{T} \tag{13}$$

is employed in obtaining equation (10). In the derivation, all terms involving second-order (or higher-order) couplings in viscosity and/or heat conductivity are neglected. We shall use equation (10) as our starting point for investigating linear photoacoustics in viscous flowing gas media with heat conduction. The equation is inhomogeneous as required, i.e., in the absence of an external heat source ($\epsilon = 0$), the acoustic pressure is zero everywhere in the gas medium. We aim at solving equation (10) for a flowing gas confined by a cylindrical tube with hard walls and subject to a general heat-source function: $\epsilon(r,\theta,z)$.

2.1. The Green's function method applied to sound propagation in flowing media confined by cylindrical walls accounting for external viscous forces, heat sources, and heat conductivity

In the following, we shall restrict our analysis to small-flow cases such that the pressure in the flow-dependent

term on the left-hand side of equation (10) can be replaced by the pressure at zero-flow conditions denoted $\tilde{p}_0$. This term is now an inhomogeneous term and can be moved to the right-hand side of equation (10) so as to give

$$\vec{\nabla}^2\tilde{p} + \frac{\omega^2}{c^2}(1-A)\,\tilde{p} = -4\pi\xi(\vec{r}), \tag{14}$$

with

$$\xi = -\frac{1}{4\pi}\left(\frac{p_0\gamma}{T_0 c_p c}[l_v - l_h]\,\vec{\nabla}^2\epsilon - \frac{p_0\gamma}{T_0 c_p c^2}(1-A)\left[\mathrm{i}\omega\epsilon + u_0\frac{\partial\epsilon}{\partial z}\right] + \frac{2\mathrm{i}\omega u_0}{c^2}\frac{\partial\tilde{p}_0}{\partial z}\right). \tag{15}$$

The corresponding Green's function $G(\vec{r},\vec{r}')$ is the solution to

$$\vec{\nabla}^2 G(\vec{r},\vec{r}') + \frac{\omega^2}{c^2}(1-A)G(\vec{r},\vec{r}') = -4\pi\delta\left(\vec{r}-\vec{r}'\right). \tag{16}$$

Next, multiplying equation (14) by $G(\vec{r},\vec{r}')$ and equation (16) by $\tilde{p}(\vec{r}')$ and subtracting leads to

$$\begin{aligned} &G(\vec{r}',\vec{r})\vec{\nabla}'^2\tilde{p}(\vec{r}') - \tilde{p}(\vec{r}')\vec{\nabla}'^2 G(\vec{r}',\vec{r}) \\ &= 4\pi\left[\tilde{p}(\vec{r}')\delta(\vec{r}-\vec{r}') - G(\vec{r}',\vec{r})\xi(\vec{r}')\right], \end{aligned} \tag{17}$$

where ∇' denotes differentiation with respect to primed coordinates: $\vec{r}'$. In deriving equation (17), $\vec{r}$ and $\vec{r}'$ have been interchanged as arguments to the Green's function. Dividing equation (17) by 4π and integrating over all $\vec{r}'$ space within V yields

$$\begin{aligned} &\frac{1}{4\pi}\int_V \left[G(\vec{r}',\vec{r})\vec{\nabla}'^2\tilde{p}(\vec{r}') - \tilde{p}(\vec{r}')\vec{\nabla}'^2 G(\vec{r}',\vec{r})\right]\mathrm{d}V' \\ &\quad + \int_V G(\vec{r}',\vec{r})\xi(\vec{r}')\,\mathrm{d}V' = \tilde{p}(\vec{r}), \end{aligned} \tag{18}$$

if $\vec{r}$ is inside S, otherwise the left-hand side of equation (18) is equal to zero. Furthermore, it is convenient to convert the first integral over V by an integral over S using Green's Theorem. Equation (18) then becomes

$$\begin{aligned} &\frac{1}{4\pi}\int_S \left[G(\vec{r}',\vec{r})\vec{\nabla}'\tilde{p}(\vec{r}') - \tilde{p}(\vec{r}')\vec{\nabla}' G(\vec{r}',\vec{r})\right]\,\mathrm{d}\vec{S}' \\ &\quad + \int_V G(\vec{r}',\vec{r})\xi(\vec{r}')dV' = \tilde{p}(\vec{r}), \end{aligned} \tag{19}$$

if $\vec{r}$ is inside S, otherwise the left-hand side of equation (19) is equal to zero.

2.2. Determination of the Green's function

The delta function in cylindrical coordinates can be expressed as

$$\delta(\vec{r}-\vec{r}') = \frac{1}{r}\delta(r-r')\delta(\theta-\theta')\delta(z-z'), \tag{20}$$

where r, θ, and z are the cylinder radial, azimuthal, and axial coordinates, respectively. It is convenient to choose our solution for the Green's function so as to satisfy Neumann boundary conditions at the cylinder wall. Thus, we expand $\delta(r-r')$ in terms of Bessel functions $J_m(x_{mn}r/R)$ where x_{mn} is the n'th zero point of $\mathrm{d}J_m(r)/\mathrm{d}r$, and $x_{mn} < x_{mn+1}$; $n = 1, 2, 3, \ldots$. Let us write

$$-\frac{4\pi}{r}\delta(r-r') = \sum_{n=1}^{\infty} A_{mn}J_m(x_{mn}r/R). \tag{21}$$

Multiplying equation (21) by $rJ_m(x_{mn'}r/R)$ and integrating from $r = 0$ to $r = R$ allows A_{mn} to be determined

$$A_{mn} = -\frac{8\pi}{R^2\left(1-m^2/x_{mn}^2\right)}\frac{J_m(x_{mn}r'/R)}{J_m^2(x_{mn})}, \tag{22}$$

where the orthogonality condition

$$\begin{aligned} &\int_0^R rJ_m(x_{mn}r/R)J_m(x_{mn'}r/R)\,\mathrm{d}r \\ &= \delta_{nn'}\frac{R^2}{2}\left(1-m^2/x_{mn}^2\right)J_m^2(x_{mn}) \end{aligned} \tag{23}$$

has been used. In equation (23), $\delta_{nn'}$ is the Kronecker delta function. We also make use of the fact that

$$\delta(\theta-\theta') = \frac{1}{2\pi}\sum_{m=-\infty}^{\infty}\exp\left(\mathrm{i}m[\theta-\theta']\right). \tag{24}$$

With the results obtained in equations (21), (22), and (24), we can express the Green's function as

$$G(\vec{r},\vec{r}') = -\frac{4}{R^2}\sum_{m=-\infty}^{\infty}\sum_{n=1}^{\infty}\frac{\exp(\mathrm{i}m[\theta-\theta'])}{\left(1-m^2/x_{mn}^2\right)}\frac{J_m(x_{mn}r/R)J_m(x_{mn}r'/R)}{J_m^2(x_{mn})}g_{mn}(z,z'), \tag{25}$$

where g_{mn} must be specified such that $G(\vec{r},\vec{r}')$ is a solution to equation (16). Notice that the expression given by equation (25) ensures that $G(\vec{r},\vec{r}')$ is a single-valued function in θ (θ') as θ (θ') changes by 2π. In addition, $G(\vec{r},\vec{r}')$ satisfies Neumann boundary conditions at the cylinder wall $r = R$ and is finite at $r = 0$ as requested.

Next, inserting equation (25) in equation (16) and using the fact that J_m is a Bessel function of order m, i.e.,

$$\left[\frac{1}{r}\frac{\partial}{\partial r}\left(r\frac{\partial}{\partial r}\right) + \left(\frac{x_{mn}^2}{R^2} - \frac{m^2}{r^2}\right)\right]J_m(x_{mn}r/R) = 0, \tag{26}$$

shows that equation (16) is fulfilled if g_{mn} is a solution to the differential equation

$$\left[\frac{\omega^2}{c^2}(1-A) - \frac{x_{mn}^2}{R^2} + \frac{\partial^2}{\partial z^2}\right]g_{mn}(z,z') = \delta(z-z'). \tag{27}$$

In the next two sections we consider two specific cases. First, we assume that the cylinder is infinitely long, e.i., we model a situation where the length is large compared to the radius. In the second case, we take into account the finite length of the cylinder assuming the end surfaces to be open (open flange condition). For completeness, we give in the appendix the Green's function for the case of a finite cylinder with hard-wall flanges although we will not consider this case in this article.

3. Determination of the photoacoustic pressure in an infinite-length cylinder with hard walls

In the case of an infinitely long cylinder the solution to equation (27) is

$$\begin{aligned} g_{mn}(z,z') &= B_{mn}\exp\left(\mathrm{i}k_{mn}[z-z']\right); \qquad z \le z', \\ g_{mn}(z,z') &= B_{mn}\exp\left(\mathrm{i}k_{mn}[z'-z]\right); \qquad z \ge z', \\ k_{mn} &= \sqrt{\frac{\omega^2}{c^2}\left(1-A\right)-\frac{x_{mn}^2}{R^2}}, \end{aligned} \tag{28}$$

where B_{mn} is a constant determined by the discontinuity jump in the derivative of g_{mn} at $z = z'$,

$$\left.\frac{\mathrm{d}g_{mn}}{\mathrm{d}z}\right|_{(z=z'+)} - \left.\frac{\mathrm{d}g_{mn}}{\mathrm{d}z}\right|_{(z=z'-)} = 1. \tag{29}$$

Equation (29) can be solved immediately so as to give

$$B_{mn} = -\frac{1}{2ik_{mn}}. \tag{30}$$

The Green's function $G(\vec{r},\vec{r}')$ can finally be expressed as

$$\begin{aligned} G(\vec{r},\vec{r}') &= \frac{2}{\mathrm{i}R^2}\sum_{m=-\infty}^{\infty}\sum_{n=1}^{\infty}\frac{\exp\left(\mathrm{i}m[\theta-\theta']\right)}{\left(1-m^2/x_{mn}^2\right)} \\ &\quad\cdot\frac{J_m(x_{mn}r/R)J_m(x_{mn}r'/R)}{J_m^2(x_{mn})}\frac{\exp\left(\mathrm{i}k_{mn}[z-z']\right)}{k_{mn}}; \\ &\qquad\qquad z \le z' \\ G(\vec{r},\vec{r}') &= \frac{2}{\mathrm{i}R^2}\sum_{m=-\infty}^{\infty}\sum_{n=1}^{\infty}\frac{\exp\left(\mathrm{i}m[\theta-\theta']\right)}{\left(1-m^2/x_{mn}^2\right)} \\ &\quad\cdot\frac{J_m(x_{mn}r/R)J_m(x_{mn}r'/R)}{J_m^2(x_{mn})}\frac{\exp\left(\mathrm{i}k_{mn}[z'-z]\right)}{k_{mn}}; \\ &\qquad\qquad z \ge z'. \end{aligned} \tag{31}$$

Employing the Green's function obtained in equation (31) allows equation (19) to be recast as

$$\tilde{p}(\vec{r}) = \int_V G(\vec{r}',\vec{r})\xi(\vec{r}')\,\mathrm{d}V', \tag{32}$$

since the pressure-gradient normal component is zero at the cylinder wall and our Green's function obeys Neumann conditions.

3.1. Photocoustic pressure in an infinite cylinder at zero flow - heating function ξ dependent on the radial coordinate only

The assumption will first be made that the heating function ξ is independent of z, θ and only a function of the radial coordinate r relevant for the situation where a long, thin light beam heats up the cylinder with the beam centered around the cylinder axis and assuming the light intensity changes infinitesimally with increasing z.

As a first step, we derive an expression for the acoustic pressure in the absence of flow. Evaluating equation (32) using equations (15) and (31) for $u_0 = 0$ yields (reintroducing the time factor $e^{\mathrm{i}\omega t}$ left out in previous sections):

$$\begin{aligned} \tilde{p}_0(r,t) &= -\frac{8\pi\mathrm{e}^{\mathrm{i}\omega t}}{R^2}\sum_{n=1}^{\infty}\frac{J_0(x_{0n}r/R)}{k_{0n}^2J_0^2(x_{0n})} \\ &\quad\cdot\int_0^R \mathrm{d}r'r'\xi r')J_0(x_{0n}r'/R), \\ \xi(r) &= -\frac{1}{4\pi}\left[\frac{p_0\gamma}{T_0c_pc}\left(l_v-l_h\right)\left(\frac{\partial^2}{\partial r^2}+\frac{1}{r}\frac{\partial}{\partial r}\right)\epsilon(r)\right. \\ &\quad\left.-\frac{p_0\gamma}{T_0c_pc^2}(1-A)\mathrm{i}\omega\epsilon(r)\right]. \end{aligned} \tag{33}$$

In succession, we can now conclude that the pressure in the presence of flow $\tilde{p}$ equals $\tilde{p}_0$ everywhere in the medium since both $\tilde{p}_0$ and ϵ are independent of z. The latter result implies that the flow-dependent terms in equation (15) vanish! In other words, a background flow will not alter the acoustic pressure if the light beam intensity is independent of the axial coordinate z.

3.2. Photocoustic pressure in an infinite cylinder at zero flow - heating function ξ dependent on the axial coordinate only

Consider next the case where the heating function ϵ is a function of z only. In this case, by evaluating equation (32), the following simple expression for the acoustic pressure is obtained at zero-flow conditions,

$$\begin{aligned} \tilde{p}_0(z,t) &= \frac{2\pi\mathrm{e}^{\mathrm{i}\omega t}}{\mathrm{i}k_{01}}\left[\int_{-\infty}^{z}\mathrm{e}^{\mathrm{i}k_{01}(z'-z)}\xi(z')\,\mathrm{d}z'\right. \\ &\quad\left.+\int_z^{\infty}\mathrm{e}^{k_{01}(z-z')}\xi(z')\,\mathrm{d}z'\right], \\ \xi(z) &= -\frac{1}{4\pi}\left[\frac{p_0\gamma}{T_0c_pc}\left(l_v-l_h\right)\frac{\partial^2\epsilon(z)}{\partial z^2}\right. \\ &\quad\left.-\frac{p_0\gamma}{T_0c_pc^2}(1-A)\mathrm{i}\omega\epsilon(z)\right], \end{aligned} \tag{34}$$

where the equation

$$\int_0^R \mathrm{d}r'r'\xi(z')J_0(x_{0n}r'/R) = \delta_{n1}\frac{R^2}{2}\xi(z'), \tag{35}$$

has been used. The latter integral result explains why $n = 1$ is the only term contributing to the infinite sum over n in equation (33).

Having determined the acoustic pressure at zero flow, we can immediately write down an expression for the pressure in the presence of flow,

$$\begin{aligned} \tilde{p}(z,t) &= \frac{2\pi\mathrm{e}^{\mathrm{i}\omega t}}{\mathrm{i}k_{01}}\left[\int_{-\infty}^{z}\mathrm{e}^{\mathrm{i}k_{01}(z'-z)}\xi(z')\,\mathrm{d}z'\right. \\ &\quad\left.+\int_z^{\infty}\mathrm{e}^{\mathrm{i}k_{01}(z-z')}\xi(z')\,\mathrm{d}z'\right], \\ \xi &= -\frac{1}{4\pi}\left[\frac{p_0\gamma}{T_0c_pc}\left(l_v-l_h\right)\frac{\partial^2\epsilon(z)}{\partial z^2}\right. \\ &\quad\left.-\frac{p_0\gamma}{T_0c_pc^2}(1-A)\left(\mathrm{i}\omega\epsilon(z)+u_0\frac{\partial\epsilon}{\partial z}\right)+\frac{2\mathrm{i}\omega u_0}{c^2}\frac{\partial\tilde{p}_0}{\partial z}\right]. \end{aligned} \tag{36}$$

4. Green's function for a finite-length hard-wall cylinder with open flanges

In this section we determine Green's function for a finite-length hard-wall cylinder with open flanges. Imposing the four conditions: (1) $g_{mn}(z = 0, z') = 0$, (2) $g_{mn}(z = L, z') = 0$, (3) $g_{mn}|_{(z=z'-)} = g_{mn}|_{(z=z'+)}$, and (4) $\mathrm{d}g_{mn}/\mathrm{d}z|_{(z=z'+)} - \mathrm{d}g_{mn}/\mathrm{d}z|_{(z=z'-)} = 1$, where $z = 0$ and $z = L$ denote the left- and right-end axial positions of the cylinder, respectively, leads to the following expression for the axial part of the Green's function

$$\begin{aligned} g_{mn}(z, z') &= \frac{1}{k_{mn}\sin\left(k_{mn}L\right)} \\ &\quad \cdot \sin\left(k_{mn}(z' - L)\right)\sin\left(k_{mn}z\right); \qquad z \le z', \\ g_{mn}(z, z') &= \frac{1}{k_{mn}\sin\left(k_{mn}L\right)} \\ &\quad \cdot \sin\left(k_{mn}(z - L)\right)\sin\left(k_{mn}z'\right); \qquad z \ge z'. \end{aligned} \tag{37}$$

Inserting equation (37) for the axial part of the Green's function in equation (25) gives the expression for the complete finite-length hard-wall cylinder Green's function with open flanges.

4.1. Photocoustic pressure in a finite cylinder at zero flow - heating function ξ dependent on the radial coordinate only

Employing the Green's function in equation (37) and equation (32) allows us to determine the acoustic pressure in the absence of flow for a heating function dependent on the radial coordinate only,

$$\begin{aligned} \tilde{p}_0(r, z, t) &= -\frac{8\pi \mathrm{e}^{\mathrm{i}\omega t}}{R^2}\sum_{n=1}^{\infty}\frac{J_0(x_{0n}r/R)}{k_{0n}^2 J_0^2(x_{0n})} \\ &\quad \cdot \frac{\sin(k_{0n}L) + \sin(k_{0n}(z - L)) - \sin(k_{0n}z)}{\sin(k_{0n}L)} \\ &\quad \cdot \int_0^R \mathrm{d}r' r' \xi(r') J_0(x_{0n}r'/R), \\ \xi(r) &= -\frac{1}{4\pi}\left[\frac{p_0\gamma}{T_0 c_p c}\left(l_v - l_h\right)\left[\frac{\partial^2}{\partial r^2} + \frac{1}{r}\frac{\partial}{\partial r}\right]\epsilon(r) \right. \\ &\quad \left. - \frac{p_0\gamma}{T_0 c_p c^2}(1 - A)\mathrm{i}\omega\epsilon(r)\right]. \end{aligned} \tag{38}$$

Note that the acoustic pressure is now dependent on the axial coordinate for the monofrequency excitation case. Due to this the pressure in the presence of flow will differ from the zero flow case.

4.2. Photocoustic pressure in a finite cylinder at zero flow - heating function ξ dependent on the axial coordinate only

Employing again the Green's function in equation (37) and equation (32) allows us to determine the acoustic pressure in the absence of flow for a heating function dependent on the axial coordinate only,

$$\begin{aligned} \tilde{p}_0(z, t) &= -\frac{4\pi \mathrm{e}^{\mathrm{i}\omega t}}{k_{01}\sin(k_{01}L)} \\ &\quad \cdot \left[\sin\left(k_{01}(z - L)\right)\int_0^z \sin\left(k_{01}z'\right)\xi(z')\,\mathrm{d}z' \right. \\ &\quad \left. + \sin\left(k_{01}z\right)\int_z^L \sin\left(k_{01}(z' - L)\right)\xi(z')\,\mathrm{d}z'\right], \\ \xi(z) &= -\frac{1}{4\pi}\left[\frac{p_0\gamma}{T_0 c_p c}\left(l_v - l_h\right)\frac{\partial^2\epsilon(z)}{\partial z^2} \right. \\ &\quad \left. - \frac{p_0\gamma}{T_0 c_p c^2}(1 - A)\mathrm{i}\omega\epsilon(z)\right]. \end{aligned} \tag{39}$$

5. Numerical Results and Discussions

In this section, we consider flowing air confined by a cylindrical tube (see Figure 1). The parameters for air are: $c_p = 1005$ J/kg/K, $K = 0.0257$ W/m/K, $\gamma = 1.4$, $T_0 = 300$ K, $\mu = 1.858 \cdot 10^{-5}$ kg/m/s, $\eta = 0$, $\rho_0 = 1.18$ kg/m^3, and $c = 347$ m/s. The cylinder radius is assumed to be $R = 0.01$ m. In the first case, we consider the heating function to be Gaussian-shaped in the radial coordinate r centered at $r = 0$ (see Figure 1, left plot)

$$\epsilon = \epsilon_{coef}\exp\left(-\frac{r^2}{2\sigma^2}\right), \tag{40}$$

which corresponds to the case where heat (light) absorption in the gas is so small that it does not lead to a drop in the heat (light) intensity as a function of the distance from heat (light) source. In other words, ϵ is independent of the axial coordinate z. In equation (40), σ denotes the broadening of the Gaussian. The coefficient ϵ_{coef} is chosen so as to normalize the Gaussian over the cylinder cross-sectional area.

Figures 2–4 refer to a photoacoustic cylinder of infinite length.

In Figure 2 (upper plot), the absolute value of the pressure amplitude at the wall ($r = R$) as a function of frequency in the range $15 - 60$ kHz is shown corresponding to a broadening factor $\sigma = 0.01$ m. The pressure amplitude denotes the total pressure apart from the $\mathrm{e}^{\mathrm{i}\omega t}$ factor. Evidently three peaks are observed corresponding to the three first resonance frequencies where the real parts of $k_{01}^2, k_{02}^2, k_{03}^2$ become zero, respectively, such that the factor $\frac{1}{k_{0n}^2}$ in equation (33) reaches its maximum value. In Figure 2 (middle and lower plots) similar frequency curves are shown for the σ values: 0.005 m and 0.002 m, respectively. Note that the pressure is independent of axial position and also independent of the background air flow.

Next, we consider the case where the heating function depends on z only (see Figure 1 (right plot)). The heating function now obeys

$$\epsilon = \epsilon_{coef}\exp\left(-\frac{z^2}{2\sigma^2}\right), \tag{41}$$

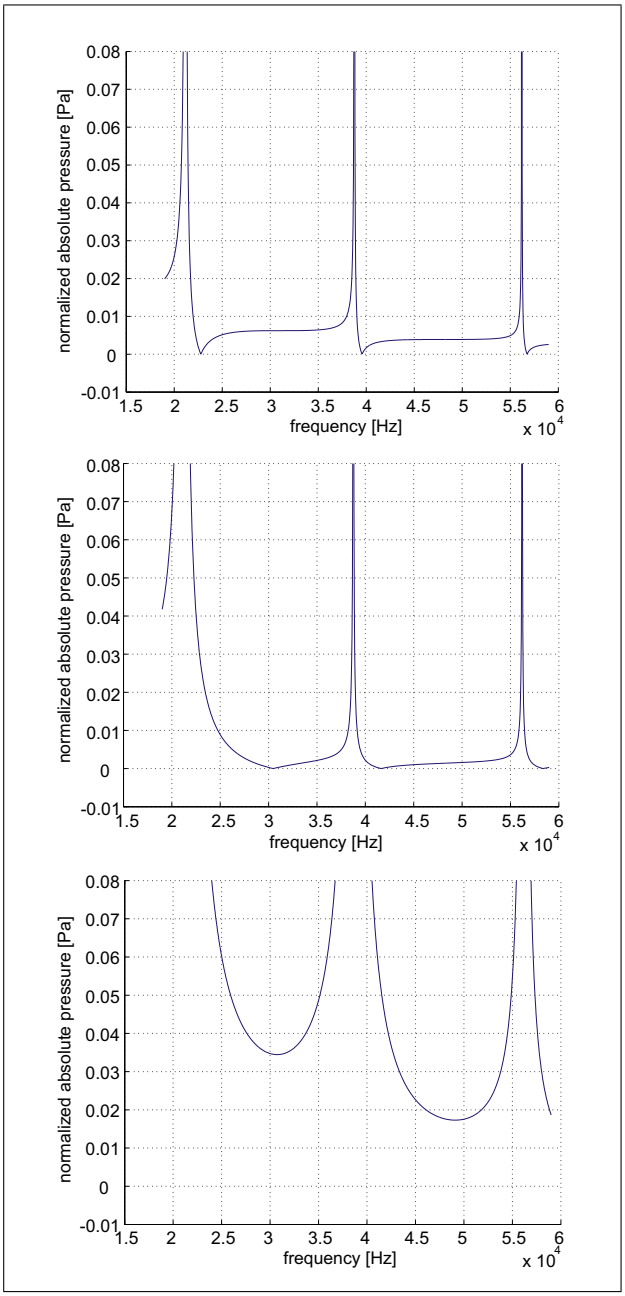

Figure 2. Plots of the absolute pressure amplitude of an infinite cylinder at the wall ($r = R$) as a function of frequency for three values of the Gaussian broadening factor: (upper) $\sigma = 0.01$ m, (middle) $\sigma = 0.005$ m, and (lower) $\sigma = 0.002$ m. The heating function is a function of the radial coordinate r only. The parameters used in the calculation and discussions are given in the Section: Numerical Results and Discussions.

corresponding to the case where the heat (light) beam is directed along the cross-section of the cylinder and centered at $z = 0$. We choose $\epsilon_{coef} = 1$ in the following. Further, it is assumed that the absorption is negligible such that the heat intensity does not depend on the radial coordinate. With a z dependence in the heating function it follows that the pressure becomes dependent on z but not r. Moreover, the pressure now depends on the background flow as mentioned in the previous section. All other computational parameters are chosen to be the same as in the example with a r-dependent heating function.

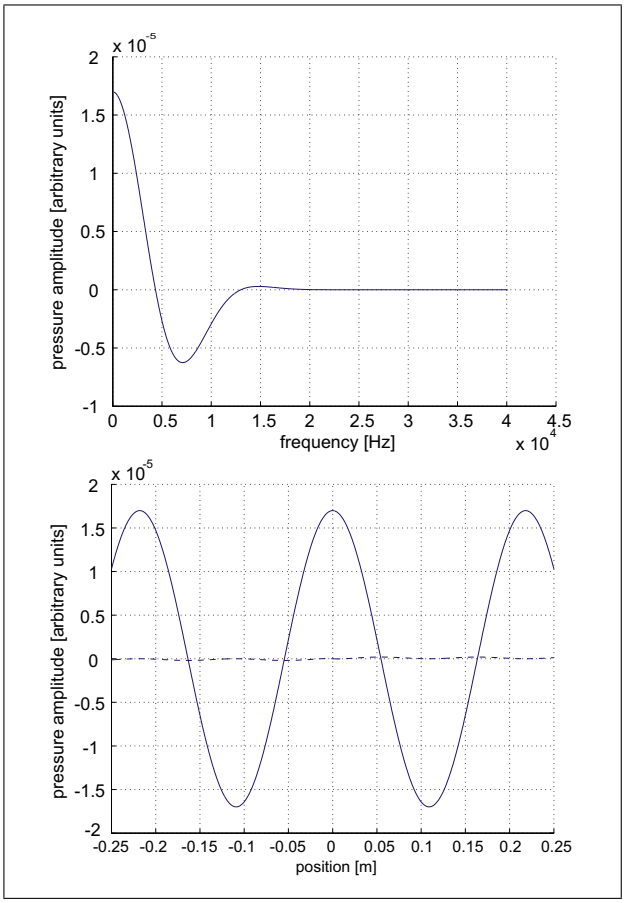

Figure 3. Plots of the real pressure amplitude of an infinite cylinder at the wall with $z = 0.02$ m as a function of frequency (in the absence of flow) for a Gaussian broadening factor: $\sigma = 0.01$ m (upper plot). In the lower plot the real part of the pressure amplitude is plotted in the absence of flow (solid) and the change in the real part of the pressure amplitude (dashed) due to a constant flow velocity $u_0 = 1$ m/s The heating function is a function of the axial coordinate z only. The parameters used in the calculation and discussions are given in the Section: Numerical Results and Discussions.

In Figure 3 (upper plot), the real part of the pressure amplitude at position $z = 0.02$ m in the absence of a background flow is shown as a function of frequency in the range: $0 - 45$ kHz for a Gaussian broadening function $\sigma = 0.01$ m.

In Figure 3 (lower plot), the real part of the pressure amplitude is plotted vs. axial distance at a frequency $10^4/2\pi$ Hz. The solid curve shows the pressure amplitude in the absence of a background flow while the dashed curve depicts the change in pressure amplitude induced by a constant flow velocity $u_0 = 1$ m/s (hence, the real part of the total pressure amplitude in the presence of a background flow is the sum of the solid and dashed curves). The Gaussian broadening function is $\sigma = 0.01$ m. The change in pressure amplitude is approximately two orders of magnitude smaller than the pressure amplitude in the absence of flow.

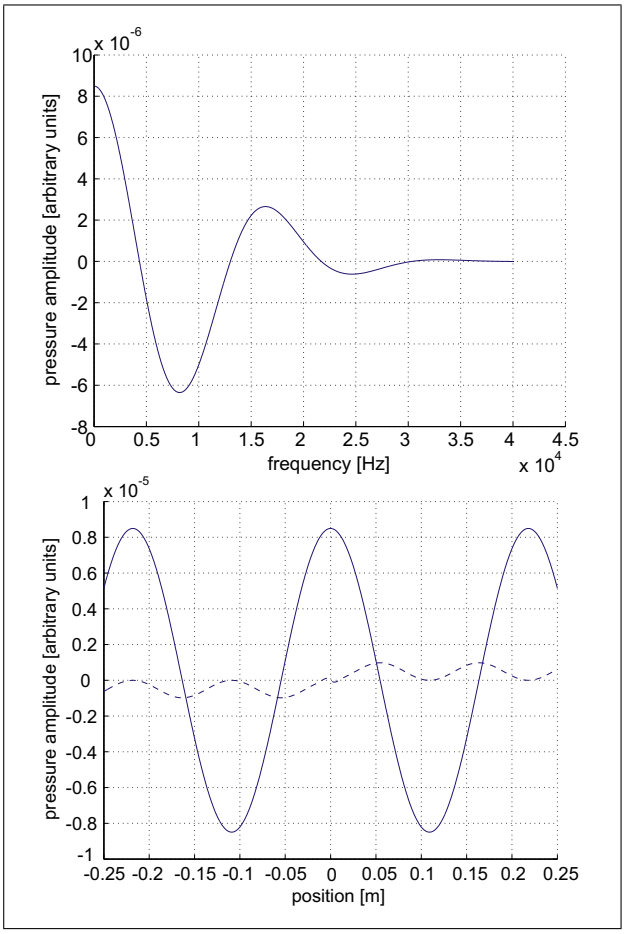

Figure 4. Plots of the real pressure amplitude of an infinite cylinder at the wall with $z = 0.02$ m as a function of frequency (in the absence of flow) for a Gaussian broadening factor: $\sigma = 0.005$ m (upper plot). In the lower plot the real part of the pressure amplitude is plotted in the absence of flow (solid) and the change in the real part of the pressure amplitude (dashed) due to a constant flow velocity $u_0 = 10$ m/s The heating function is a function of the axial coordinate z only. The parameters used in the calculation and discussions are given in the Section: Numerical Results and Discussions.

In Figure 4 (upper plot), the real part of the pressure amplitude is shown at position $z = 0.02$ m and $r = R$ in the absence of a background flow as a function of frequency in the range: $0 - 45$ kHz for a Gaussian broadening function $\sigma = 0.005$ m. In Figure 4 (lower plot), the real part of the pressure amplitude is plotted vs. axial distance in the presence of a constant flow $u_0 = 10$ m/s at a frequency $\frac{10^4}{2\pi}$ Hz. The solid curve shows the pressure amplitude in the absence of a background flow while the dashed curve depicts the change in pressure amplitude induced by a constant flow velocit y $u_0 = 1$ m/s (again, the real part of the total pressure amplitude in the presence of a background flow is the sum of the solid and dashed curves). The Gaussian broadening function is $\sigma = 0.005$ m. The change in pressure amplitude is approximately one order of magnitude smaller than the pressure amplitude in the absence of flow.

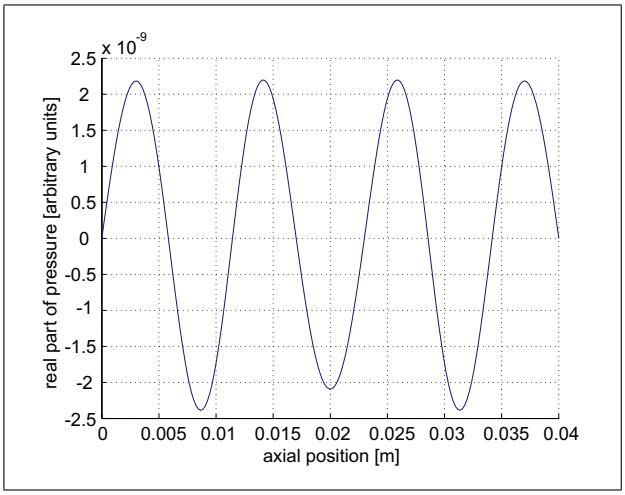

Figure 5. Plot of the real part of the acoustic pressure amplitude in the absence of flow for a cylinder with open flanges at $z = 0$ and $z = L$ [using equation (38)]. The Gaussian broadening factor is $\sigma = 0.002$ m for a heating function dependent on the radial coordinate only. Other parameters used in the calculation are given in the Section: Numerical Results and Discussions.

In the Figures 5–7, we consider a photoacoustic cylinder of finite length ($L = 0.04$ m) with open flanges at the cylinder end positions: $z = 0$ and $z = L$.

In Figure 5, a plot of the real part of the acoustic pressure amplitude in equation (38) [corresponding to $u_0 = 0$] is shown. Parameters used are: $\frac{\omega}{2\pi} = 5 \cdot 10^4$ Hz, $\sigma = 0.002$ m, and ϵ_{coef} is normalized such that the heating function integrated over the cross-sectional area is 1. Observe that since

$$\sin\left(k_{0n}(z-L)\right) - \sin\left(k_{0n}z\right) = -2\cos\left(k_{0n}(z-L/2)\right)\sin\left(k_{0n}L/2\right), \quad (42)$$

it follows that the pressure is always symmetric with respect to the center of the cylinder $z = L/2$.

The approximation where the acoustic pressure was replaced with the zero flow pressure in one of the terms of equation (10) in order to arrive at equation (14) has been checked against finite element calculations in the framework of COMSOL Multiphysics. Furthermore, using the finite element model we have investigated the dependence of the acoustic pressure on different flow profiles. This problem is tractable using the finite-element method for any flow profile. A Green's function analysis, on the other hand, suffers from being rather cumbersome for a general flow-profile.

In Figure 6, the logarithm of the absolute real part of the acoustic pressure is plotted as a function of frequency at two points along the surface of the cylinder. The light is assumed to be incident along the tube, i.e., the heating function is only dependent on r, and $\sigma = 0.002$ m. For the upper plot the flow is zero, the middle plot shows the behavior for a constant flow with $u_0 = 5$ m/s, and the

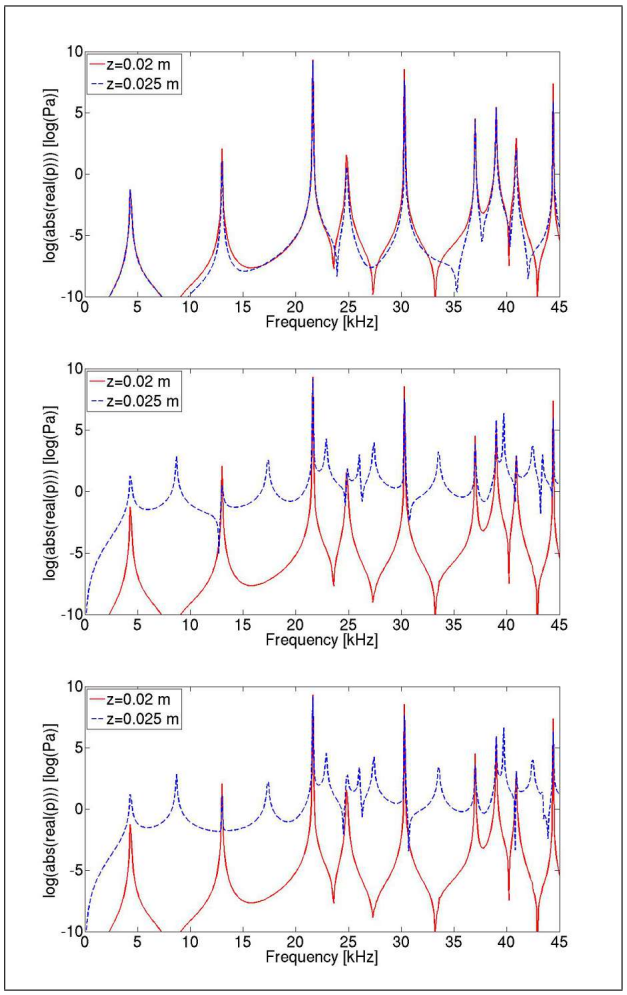

Figure 6. Plots of the logarithm of the absolute real part of the acoustic pressure as a function of frequency along the wall for zero flow (upper), constant flow (middle), and a parabolic flow profile (lower). The pressure is given at the two points $z = 0.02$ m and $z = 0.025$ m. The Gaussian broadening factor is $\sigma = 0.002$ m for a heating function dependent on r only. The pipe is finite with $L = 0.04$ m and has open flanges.

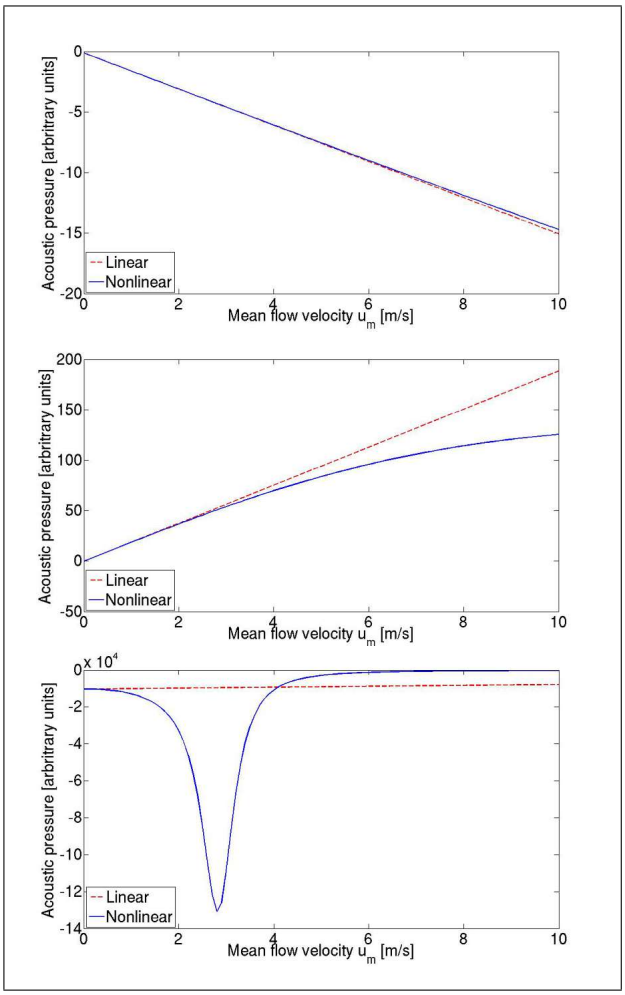

Figure 7. Plots of the real part of the acoustic pressure as a function of mean flow velocity at the surface of the pipe at $z = 0.025$ m. The upper plot is at 22 kHz, the middle plot is at 22.6 kHz, and the lower plot is at 21.35 kHz. The solid lines are results based on the linear model and the dashed lines are results where some nonlinearities have been included (refer to the main text). The Gaussian broadening factor is $\sigma = 0.002$ m for a heating function dependent on r only. The pipe is finite with $L = 0.04$ m and has open flanges.

lower plot illustrates the behavior for a parabolic flow profile with a mean flow velocity of $u_m = 5$ m/s, i.e.,

$$u_0 = 2u_m\left(1 - \frac{r^2}{R^2}\right). \tag{43}$$

From these plots we see that additional peaks appear when flow is present. This is not the case for an infinite pipe where no influence of the flow on the acoustic pressure is found neglecting a decreasing laser-beam intensity as a function of z due to absorption. The reason we see additional peaks in the finite-cylinder case with flow is that open flanges introduce a z dependence of the acoustic pressure. Furthermore, we see that the acoustic pressure contributions from the additional peaks are zero at the center of the resonator ($z = 0.02$ m). We do not see any significant difference between the two profiles. This indicates that the exact flow profile does not influence results much.

The appearance and strength of these new peaks is surprising and the question arises whether a linear theory with respect to the flow velocity is sufficient at the fairly high velocities we are considering. A complete investigation of nonlinear contributions is outside the scope of this article, however, we have investigated the influence of keeping the $\frac{\partial \tilde{p}}{\partial z}$ term in equation (10). In Figure 7, we show the acoustic pressure at the surface of the pipe at $z = 0.025$ m as a function of the mean flow velocity for three frequencies. The first frequency (22 kHz) is chosen off resonance. Here we see only small deviations due to nonlinearities in the mean flow u_0. The second frequency (22.9 kHz) is chosen at one of the "new", i.e., flow-induced, peaks. At this frequency, we observe significant deviations around 6 m/s. Finally, the third frequency (21.6 kHz) is chosen at one of the resonances appearing already at zero flow. Here, the linear-in-mean-flow model deviates significantly even at 1 m/s. From this we conclude the following. First of all, the accuracy of the linear approximation depends

strongly on the frequency (further discussions on nonlinearities and flow can be found in, e.g., Ref. [14]). Secondly, for small flows, the linear-in-mean-flow approximation works well at all frequencies (this is expected), however, deviations appear already near 1% of the speed of sound. It is important to emphasize that the finite-element analysis presented explains when the linear-in-mean-flow approach breaks down but does not provide information as to the quantitative influence of nonlinear effects. This is a consequence of the fact that we have not accounted for all nonlinearities to a given order in deriving equation (10). This will be the focus of a forthcoming paper.

6. Conclusions

A wave equation is derived describing photoacoustics in a flowing, viscous, and thermal-conducting medium. Sound excitation is due to a localized heating source. The Green's function method is used to analytically determine the acoustic pressure in the presence of a constant gas flow, i.e., independent of the cylinder radial coordinate. Next, several test cases corresponding to various boundary conditions are solved showing the dependence of the acoustic pressure vs. a constant gas flow. Finally, finite-element based results for the photoacoustic pressure are presented with emphasis to changes in photoacoustic-resonator frequencies as a function of mean flow and flow profile. It is shown that flow gives rise to additional peaks and pointed out that nonlinearities become significant even for velocities as low as 1% of the speed of sound.

Appendix

Green's function for a finite-length hard-wall cylinder with hard-wall flanges

In this section we determine Green's function for a finite-length hard-wall cylinder. Imposing the four conditions: (1) $\mathrm{d}g_{mn}(z=0,z')/\mathrm{d}z=0$, (2) $\mathrm{d}g_{mn}(z=L,z')/\mathrm{d}z=0$, (3) $g_{mn}|_{(z=z'-)}=g_{mn}|_{(z=z'+)}$, and (4) $\mathrm{d}g_{mn}/\mathrm{d}z|_{(z=z'+)}-\mathrm{d}g_{mn}/\mathrm{d}z|_{(z=z'-)}=1$, where $z=0$ and $z=L$ denote the left- and right-end axial positions of the cylinder, respectively, leads to the following expression for the axial part of the Green's function

$$\begin{aligned} g_{mn}(z,z') &= \frac{1}{k_{mn}\sin\left(k_{mn}L\right)} \\ &\quad \cos\left(k_{mn}(z'-L)\right)\cos\left(k_{mn}z\right); \qquad z\le z', \\ g_{mn}(z,z') &= \frac{1}{k_{mn}\sin\left(k_{mn}L\right)} \\ &\quad \cos\left(k_{mn}(z-L)\right)\cos\left(k_{mn}z'\right); \qquad z\ge z'. \end{aligned} \tag{A1}$$

Inserting equation (A1) for the axial part of the Green's function in equation (25) gives the expression for the complete finite-length hard-wall cylinder Green's function.

Photocoustic pressure in a finite cylinder at zero flow - heating function ξ dependent on the radial coordinate only

Employing the Green's function in equation (A1) and equation (32) allows us to determine the acoustic pressure in the absence of flow for a heating function dependent on the radial coordinate only,

$$\begin{aligned} \tilde{p}_0(r,t) &= -\frac{8\pi \mathrm{e}^{\mathrm{i}\omega t}}{R^2}\sum_{n=1}^{\infty}\frac{J_0(x_{0n}r/R)}{k_{0n}^2J_0^2(x_{0n})} \\ &\quad \cdot\int_0^R \mathrm{d}r' r'\xi(r')J_0(x_{0n}r'/R), \\ \xi(r) &= -\frac{1}{4\pi}\left[\frac{p_0\gamma}{T_0c_pc}\left[l_v-l_h\right]\left[\frac{\partial^2}{\partial r^2}+\frac{1}{r}\frac{\partial}{\partial r}\right]\epsilon(r)\right. \\ &\quad \left. -\frac{p_0\gamma}{T_0c_pc^2}(1-A)\mathrm{i}\omega\epsilon(r)\right]. \end{aligned} \tag{A2}$$

Note that the acoustic pressure is independent of the axial coordinate for a monofrequency light excitation case independent of the axial coordinate.

Photocoustic pressure in a finite cylinder at zero flow - heating function ξ dependent on the axial coordinate only

Employing again the Green's function in equation (A1) and equation (32) allows us to determine the acoustic pressure in the absence of flow for a heating function dependent on the axial coordinate only,

$$\begin{aligned} \tilde{p}_0(z,t) &= -\frac{4\pi \mathrm{e}^{\mathrm{i}\omega t}}{k_{01}\sin\left(k_{01}L\right)} \\ &\quad \cdot\left[\cos\left(k_{01}(z-L)\right)\int_0^z\cos\left(k_{01}z'\right)\xi(z')\,\mathrm{d}z'\right. \\ &\quad \left.+\cos\left(k_{01}z\right)\int_z^L\cos\left(k_{01}(z'-L)\right)\xi(z')\,\mathrm{d}z'\right], \\ \xi(z) &= -\frac{1}{4\pi}\left[\frac{p_0\gamma}{T_0c_pc}\left[l_v-l_h\right]\frac{\partial^2\epsilon(z)}{\partial z^2}\right. \\ &\quad \left.-\frac{p_0\gamma}{T_0c_pc^2}(1-A)\mathrm{i}\omega\epsilon(z)\right]. \end{aligned} \tag{A3}$$

Note that this time the acoustic pressure is independent of the radial coordinate but generally a function of the axial coordinate.

Acknowledgement

We are grateful to Lars Duggen for a careful reading of the manuscript.

References

[1] F. J. M. Harren, G. Cotti, J. Oomens, S. te Lintel Hekkert: Photoacoustic spectroscopy in trace gas monitoring. – In: Encyclopedia of Analytical Chemistry. John Wiley & Sons Ltd, Chichester, 2000, 2203–2226.

[2] A. C. Tam. Rev. Mod. Phys. **58** (1986) 381–431.

[3] A. Karbach, P. Hess. J. Chem. Phys. **84** (1986) 2945–2952.

[4] G. J. Diebold, P. J. Westervelt. J. Acoust. Soc. Am. **84** (1988) 2245–2251.

[5] G. J. Diebold, T. Sun, M. I. Khan. Phys. Rev. Lett. **67** (1991) 3384–3387.

[6] B. T. Cox, P. C. Beard. J. Acoust. Soc. Am. **117** (2004) 3616–3627.

[7] P. M. Morse, K. U. Ingard: Theoretical acoustics. International series in pure and applied physics. McGraw-Hill, 1968.

[8] E. I. Boamfa, M. M. L. Steeghs, S. M. Cristescu, F. J. M. Harren. Int. J. Mass Spectrometry **239** (2004) 193–201.

[9] A. Miklos, P. Hess, Z. Bozoki. Rev. Sci. Instruments **72** (2001) 1937–1955.

[10] M. Willatzen. J. Sound Vib. **248** (2001) 847–863.

[11] M. Willatzen. J. Acoust. Soc. Am. **109** (2001) 102–107.

[12] M. L. Munjal, M. G. Prasad. J. Acoust. Soc. Am. **80** (1986) 1501–1506.

[13] B. Karthik, B. Manoj Kumar, R. I. Sujith. J. Acoust. Soc. Am. **108** (2000) 38–43.

[14] M. Willatzen, H. Kamath. Flow Meas. Instrum. **19** (2008) 79–84.